Cell Reports
Physical Science

CellPress
OPEN ACCESS

Article

Fluidic control programming for 3D magnetic soft metamaterials with reconfigurable mechanical behaviors

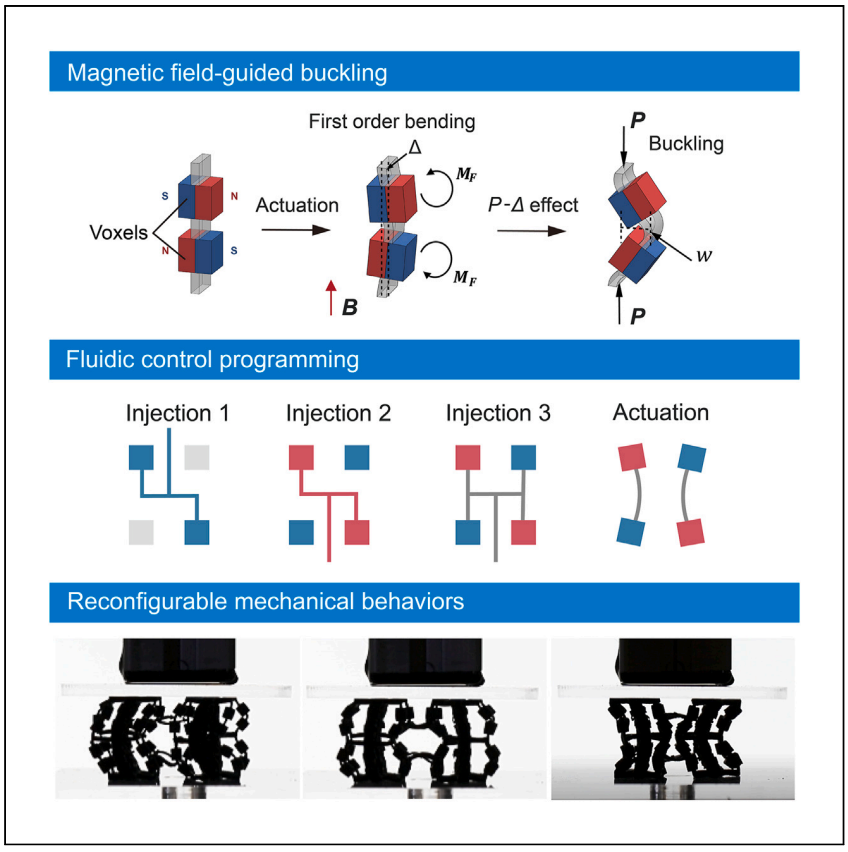

Magnetic soft materials exhibit flexible programmability, offering advancements in soft robotics and responsive devices. Several technical questions regarding the introduction of 3D magnetic configurations remain. This work introduces a fluid control programming method that precisely constructs mechanical metamaterials with 3D magnetic configurations and reconfigurable mechanical behaviors.

Zhuoyue Wang, Sarthak Misra, Venkatasubramanian Kalpathy Venkiteswaran

z.wang01@umcg.nl

Highlights

A 3D fluid injection method is established to program the magnetic configurations

Magnetic-field-guided elastic buckling is employed as the metamaterial mechanism

3D shape changing is enabled to realize reconfigurable mechanical behaviors

The potential applications for robotic and electronic devices are validated

Wang et al., Cell Reports Physical Science 5, 102125
August 21, 2024
Published by Elsevier Inc.
https://doi.org/10.1016/j.xcrp.2024.102125

Please cite this article in press as: Wang et al., Fluidic control programming for 3D magnetic soft metamaterials with reconfigurable mechanical behaviors, Cell Reports Physical Science (2024), https://doi.org/10.1016/j.xcrp.2024.102125

Cell Reports
Physical Science

CellPress
OPEN ACCESS

Article

Fluidic control programming for 3D magnetic soft metamaterials with reconfigurable mechanical behaviors

Zhuoyue Wang,[1,3,*] Sarthak Misra,[1,2] and Venkatasubramanian Kalpathy Venkiteswaran[2]

SUMMARY

Active mechanical metamaterials are an attractive proposition for soft robotics, electronic devices, and biomedical devices. However, the utilization of their uncommon physical and mechanical behaviors remains underexplored because existing fabrication processes limit the decoupling of structural frameworks from the responsive mechanisms. Here, we propose a multi-step fluidic control programming strategy by fabricating three-dimensional (3D) magnetic soft materials (MSMs) with reconfigurable mechanical metamaterial behaviors, enabling magnetic-field-driven alteration between three different geometry modes in a single structure. The MSM lattices exhibit fast 3D transitions between positive ($\nu_{max} = 3.41$) and negative ($\nu_{max} = -2.64$) Poisson's ratios. We then create MSMs with reconfigurable orthotropic behaviors, which demonstrate the positive and negative Poisson's effect in perpendicular planes. In further demonstrations, the fast and wireless response is validated by manipulating falling loads and switching the states of electrical circuits. This research provides a controllable workflow for future magnetic soft metamaterials.

INTRODUCTION

The development of intelligent technologies in industries such as automation, aerospace, electronics, and biomedicine places tremendous demand on the mechanical features of metamaterials.[1] Mechanical metamaterials with rationally designed structures offer great possibilities for programming shape change and variable macro-level material responses.[2,3] Unique properties are proven in mechanical metamaterials such as negative Poisson's ratio (auxetic),[4–7] negative stiffness,[8,9] negative thermal expansion,[10–12] and twist under compression.[13] In many of these cases, the properties remain invariable after fabrication, as they are embedded within the structure of the materials. To enable the alteration of mechanical properties after fabrication, recent advances have employed stimuli-responsive materials such as shape memory polymers,[14–18] the shape of which can be reprogrammed when heated above the critical temperature; hydrogels that can absorb or lose water molecules; and magnetic materials such as permanent magnets[19,20] and magnetic soft materials (MSMs).[21] These materials are often limited by their uniform response mode and the ability to form complex three-dimensional (3D) structures.

Due to the rapid and wireless response in external magnetic fields, MSMs have attracted widespread interest, particularly in biomedical applications.[22–28] Polydimethylsiloxane (PDMS) and Ecoflex are frequently used as the matrix for magnetic fillers, which can incorporate both soft and hard magnetic particles.[29] By implanting specific magnetization patterns into the materials, these soft materials can perform

[1]Department of Biomaterials and Biomedical Technology, University of Groningen and University Medical Centre Groningen, Groningen 9713 GZ, the Netherlands

[2]Department of Biomechanical Engineering, University of Twente, Enschede 7500 AE, the Netherlands

[3]Lead contact

*Correspondence: z.wang01@umcg.nl

https://doi.org/10.1016/j.xcrp.2024.102125

Please cite this article in press as: Wang et al., Fluidic control programming for 3D magnetic soft metamaterials with reconfigurable mechanical behaviors, Cell Reports Physical Science (2024), https://doi.org/10.1016/j.xcrp.2024.102125

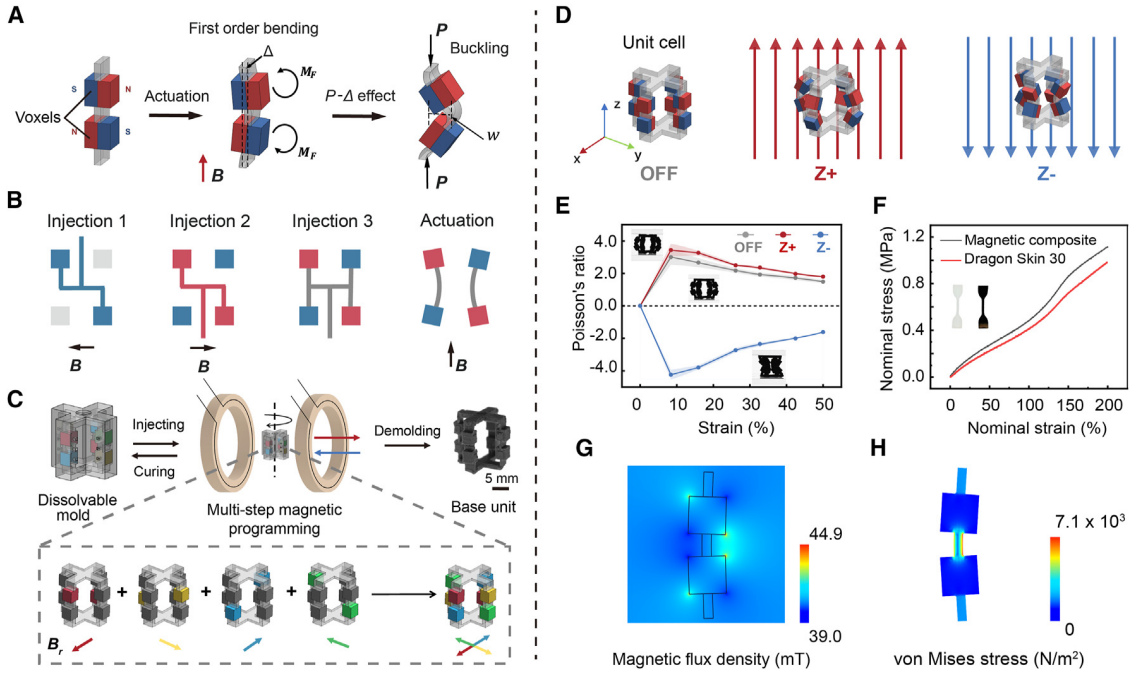

Figure 1. Design, fabrication, and mechanical behavior of the reconfigurable base unit of MSMs

(A) Schematic diagrams illustrate the mechanism of magnetic-field-guided buckling on a single beam.

(B) Schematics of the concept of multi-step injection and orientation.

(C) Iterative fluid injection programming procedure of the magnetic soft material (MSM) base unit. The directions are represented by four colors (red, yellow, blue, and green).

(D) Schematic diagrams illustrate the base unit when the external magnetic field is turned off (defined as OFF), upward (defined as z+), and downward (defined as z−).

(E) Poisson's ratio-strain curve of programmable MSM unit.

(F) Nominal stress-nominal strain curves of Dragon Skin 30 and the magnetic composite.

(G) Simulation of the magnetic flux density of one segment.

(H) Simulation of the segment under magnetic-field-driven bending.

geometric deformations, including bending,[30,31] twisting,[32] and folding.[31,33] Generally, MSMs are shaped into wires,[34] films,[35,36] cubes, origami structures,[37–39] and lattices[19,40] via various fabrication methods such as molding and casting,[41–43] additive manufacturing (3D printing),[32,33,44–46] 3D micro-assembling,[22] and reorientation of magnetic dipoles.[47,48] However, current fabrication techniques either lack the automated workflow needed to build 3D structures or cannot produce 3D magnetization patterns,[21] although the decoupling of structural fabrication and patterned magnetization is essential for introducing the necessary complexity and controllability for 3D magnetic-responsive metamaterials.

To address this challenge, we present a strategy to imbue 3D magnetization patterns into soft metamaterial structures and achieve multi-modal deformation in three dimensions. First, MSMs are designed with stimuli-responsive voxels that can be regulated for specific magnetic moments in each segment. The segments are able to show a magnetic actuation-guided elastic buckling behavior based on a second-order effect (P-Δ effect), and the buckling direction can be controlled by the direction of the magnetic field (Figures 1A and S1). To realize the individual programming of each voxel, we developed a fluidic injection technique, allowing specific voxels to be selectively filled and magnetized in disparate directions by two separate injections (Figure 1B). Subsequently, a third injection connects all voxels

Please cite this article in press as: Wang et al., Fluidic control programming for 3D magnetic soft metamaterials with reconfigurable mechanical behaviors, Cell Reports Physical Science (2024), https://doi.org/10.1016/j.xcrp.2024.102125

by filling the remaining spaces with non-magnetized composite material, ensuring structural continuity throughout the lattice.

Here, a systematic fabrication method based on multi-step injection and orientation of the particles in a weak field (80 mT) is developed. The voxel-dominated segments are magnetized and assembled in groups by the programming of fluidic injection channel and magnetic orientation procedures (Figure 1C). This approach allows multiple magnetization directions embedded in the same structure without the need for assembly afterward. By assembling the segments in a pre-defined order, magnetically programmable mechanical behaviors, for instance, switching between negative and positive Poisson's ratios, are achieved (Figure 1D). Since the composite in each step is fully cured before injection in the next step, the conflict of magnetization directions is avoided between the adjacent elements. This fluidic control programming strategy solves the integration problem of fabricating 3D structures and 3D magnetization on arbitrary directions and creates MSMs showing unique mechanical behaviors.

Due to the carefully designed structures and magnetization patterns, the metamaterials exhibit sensitive responses and perform rapid switching between negative and positive Poisson's ratios and orthotropic shape changing. This swift switching feature is further proven using a load-carrying metamaterial unit falling under gravity through a tube. We perform a series of *in situ* mechanical tests to characterize these behaviors in the presence of an upward vertical magnetic field (defined as z+) and a downward magnetic field (defined as z−) and when the magnetic field is completely switched off (defined as OFF). A demonstration of our MSM lattice shows the ability to control electrical circuits with external magnetic fields. The reconfigurability of MSMs holds great potential in advancing the field of soft robots and electronics. The advancement of this work is further illustrated by comparing it to existing studies, as shown in Table S1.

RESULTS AND DISCUSSION

Design and fabrication of reconfigurable base unit

To achieve 3D responsive deformation, we design a base unit with four segments composed of magnetically responsive voxels and linking members. In this base unit, each voxel can be magnetized in an individual direction using the fluidic control programming method developed in this study. With an alternating magnetization pattern, a lateral bending deflection is generated in the segments due to the effect of the magnetic moment. By assembling the magnetized segments, variable bending modes can be achieved. Here, we use four segments with the magnetization pattern illustrated in Figure 1A to realize MSM units with switchable Poisson's ratio behavior.

To evaluate the programmable bending behavior, we introduce the concept of magnetic-field-guided elastic buckling. Here, a programmable deformation mode of the base unit is achieved by controlling the direction of the magnetic moment via an external field and can be calculated by Equation 1:

$$\boldsymbol{M}_F = \boldsymbol{m} \times \boldsymbol{B}, \qquad \text{(Equation 1)}$$

where $\boldsymbol{M}_F$ is the magnetic torque (N · m), $\boldsymbol{m}$ is the magnetic moment (A · m^2), and $\boldsymbol{B}$ is the magnetic flux density applied (T). It is worth mentioning that the first-order bending moment is provided by the magnetic field, which also eliminates the uncertainty of the buckling direction.

When the magnetic field is turned on, each beam segment is in a slight bending equilibrium with an initial deflection Δ. The addition of a further compressive load

Please cite this article in press as: Wang et al., Fluidic control programming for 3D magnetic soft metamaterials with reconfigurable mechanical behaviors, Cell Reports Physical Science (2024), https://doi.org/10.1016/j.xcrp.2024.102125

leads to an amplification that tends to produce buckling behavior under a P-Δ effect, as described by beam-column theory[49] with the differential Equation 2:

$$EIw'''' + Pw'' = 0 \quad \text{(Equation 2)}$$

where E is the elastic modulus of the composite material (Pa), I is the polar moment of inertia of the beam on the bending axis (m^4), P is the vertical compression load (N), and w is the deflection at mid-span of the beam (m).

The base unit consists of four groups of magnetized segments, where each segment comprises two magnetic-responsive voxels, and the geometrical design is displayed in the supplemental information (Figure S2). To magnetize the voxels, we sequentially deploy four steps of material injection followed by orientating and curing in a pair of Helmholtz coils. For the base unit, each voxel is magnetized to generate a magnetic moment of equal magnitude but in the opposite direction to its neighbor.

In mechanical tests, the programmable base unit shows a tri-state mechanical behavior where its deflection mode under compression can be altered by external magnetic fields (Figures 1E and S6; supplemental information). When the external magnetic field is OFF, the unit exhibits a positive Poisson's ratio (ν_{max} = 3.47) due to the constrained mode. Instability behavior is observed with a critical load of 66 mN. A pre-deformed curvature is observed in both z+ and z− fields at a flux density of 50 mT. A positive Poisson's ratio (ν_{max} = 3.82) and a critical load of 58 mN are observed in the z+ field. The Poisson's ratio can be switched to negative (ν_{max} = −4.52) by applying a z− field with a critical load of 76 mN. Also, the unit shows a higher stiffness when the field is turned to z−. This is because, in the negative Poisson's ratio state, the voxels contact and lock each other when moving to the center of the unit, as the deformation space is compressed. For the silicone matrix, Dragon Skin 30 was selected, and other materials such as PDMS or Ecoflex are also possible. To better evaluate the magnetic-mechanical performance, tensile tests have been performed on the Dragon Skin 30 and magnetic composite samples, which are prepared according to tensile test standards. Nominal stress-nominal strain curves are shown in Figure 1F. The magnetic flux density of a two-voxel beam (one segment) bending in the presence of a 50 mT magnetic field is simulated (Figure 1G). The bending curvature and stress state of one segment in a vertical magnetic field are then simulated in Figure 1H. When fabricating a base unit, the mold is designed with nine injection inlets, allowing the 8 voxels and the connecting beams to be injected individually. However, extending this programmable mechanical property to a larger scale requires a strategy to fill and orientate multiple voxels simultaneously. To address this challenge, a systematic method to achieve desired spatial magnetic configuration is established.

Multi-step fluidic control programming and 3D magnetic orientation

Developed from traditional molding methods, the multi-step fluidic control programming involves mold fabricating, fluid injecting, and demolding procedures. Here, the mold for the multi-unit structure is initially created using a fused deposition modeling 3D printer, employing a butanediol vinyl alcohol co-polymer filament for its solubility in water. Once the 3D printing is completed, a mixture of magnetic particles and polysiloxane elastomer is injected into the mold with a precision pump in a series of iterative steps. After each injection iteration, the mold is positioned within an electromagnetic system, aligning the uncured composite along the pre-determined axis.

To evaluate the fluid properties of the composite, rheological tests are performed as shown in Figure S4. The shear-thinning behavior of the PrFeB and Dragon Skin 30

Please cite this article in press as: Wang et al., Fluidic control programming for 3D magnetic soft metamaterials with reconfigurable mechanical behaviors, Cell Reports Physical Science (2024), https://doi.org/10.1016/j.xcrp.2024.102125

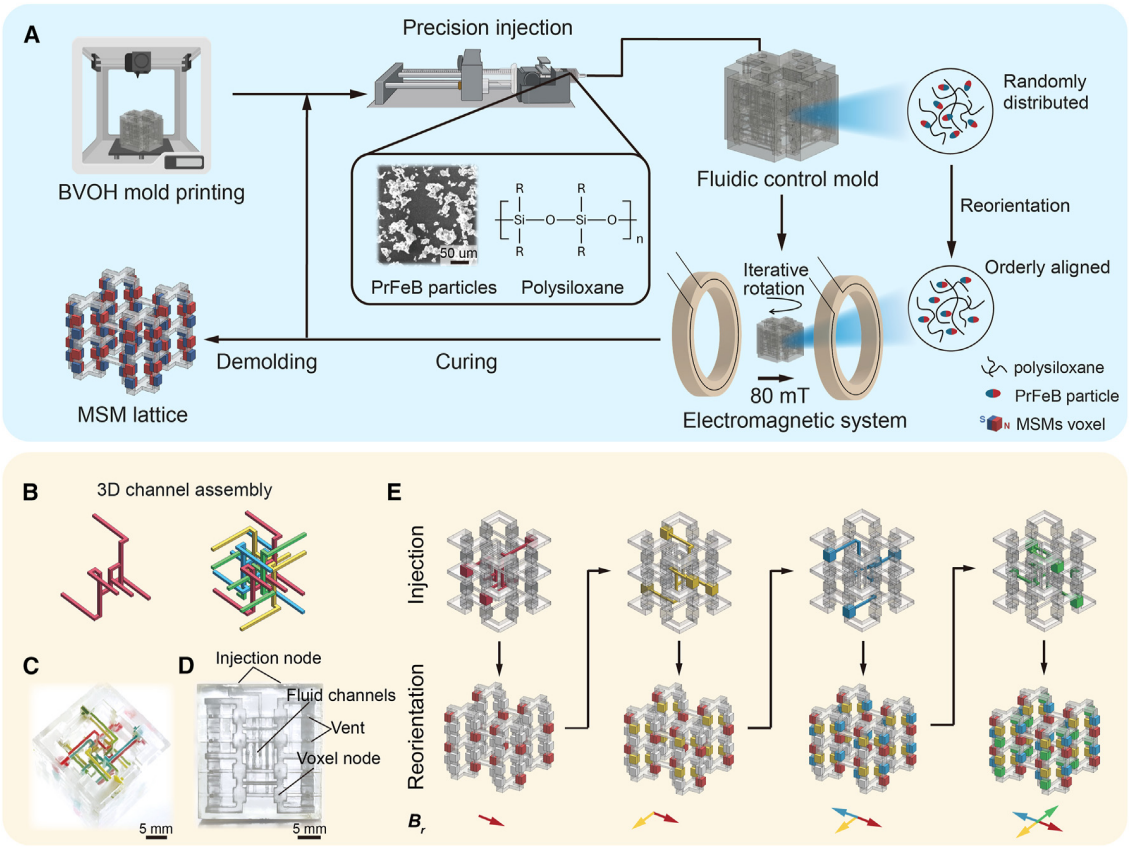

Figure 2. Fluidic control programming strategy for fabricating multi-unit MSM lattices

(A) Structural fabrication and 3D fluidic control programming procedure of multi-unit MSM lattices. The magnetic particles are characterized with scanning electron microscopy image.

(B) Structure of fluid channels used for multi-directional magnetic programming. Each magnetization iteration is represented by one of the four colors (red, yellow, blue, and green).

(C) Image of 3D-printed transparent mold injected with four distinct colors.

(D) Cross-section view image of 3D-printed transparent mold.

(E) Schematics on the 3D multi-step injection and orientation steps. The iterations are represented by four colors (red, yellow, blue, and green).

mixture facilitates smooth injection with low resistance, while its higher viscosity ensures stable particle distribution within the fluid matrix, crucial for consistent material properties and performance. The uniformity is further characterized with scanning electron microscope (Figure S5). Once the injection and magnetic alignment processes are completed, the mold undergoes a curing phase to solidify the composite. Then, the next iteration of injection, magnetization, and curing is performed on a different section of the mold. After the full array of iterations is completed, the entire mold is submerged in a hot water bath, where it is designed to dissolve completely, as depicted in Figure S7.

This approach can be extended to create MSMs with more voxels and magnetic configurations, as designed in Figure S3. To facilitate this complex injection process in a 3D scenario, we designed a 3D injection channel with one inlet and four outlet nodes. Here, this model is systematically rotated four times to assemble a comprehensive 3D fluidic programming channel model, as shown in Figure 2B. To visualize the capabilities of this fluidic control system, a transparent mold is prototyped using a stereolithography printer. This mold is then filled with four colors of pigment to

Please cite this article in press as: Wang et al., Fluidic control programming for 3D magnetic soft metamaterials with reconfigurable mechanical behaviors, Cell Reports Physical Science (2024), https://doi.org/10.1016/j.xcrp.2024.102125

differentiate and highlight the flow paths and channel configurations, as shown in Figures 2C. Figure 2D shows a cross-sectional view of this transparent mold, revealing the intricate internal structure of the fluidic control system. To further illustrate the process of fabricating the 8-unit MSM lattice with four-directional magnetic configurations, Figure 2E shows the sequential injections and corresponding magnetic reorientations.

MSM lattice with switchable Poisson's ratio

The programmable mechanical properties of the lattice are characterized in an *in situ* mechanical test system as depicted in Figure S8. This setup includes a linear slide to apply the compressive load, force sensors, and electromagnetic coils to provide switchable magnetic fields. In this study, three different magnetic environments (OFF, z+, and z−) are selected to investigate the programmable mechanical behavior of the lattices. To describe the deflection mode, we model the segments as Euler-Bernoulli beams, and the elastic beams can be described with discontinuous buckling when the non-linearity is sufficiently strong, where the value of post-buckling slope (S) indicates different buckling modes including slender beams, wide beams, and metabeams.[50]

In the uniaxial compression tests, three lateral deformation modes are observed. The process of the mechanical test is presented in Figure 3A and Video S1, with the compressive strain increasing from 0% to 30%. Finite element analysis also suggests the same deformation modes in the experiments (Figure 3B). The programmable mechanical properties are further evaluated in the load-displacement curves (Figure 3C) and strain-Poisson's ratio curves (Figure 3D). Upon removal of the magnetic field, the metamaterial lattice exhibits the instability behaviors corresponding to discontinuous buckling mode. This is evidenced in the load-displacement curve, wherein a negative slope is observed after the average critical load of 300 mN, and the Poisson's ratio stays near zero. Additionally, several instability buckling modes are observed under identical conditions (Figure S9), showing the non-linearity of the system. Due to the randomness of these buckling modes, we do not consider negative stiffness as one of the designed mechanical properties.

The instabilities are practically eliminated when the magnetic field is activated, which can be identified from the unified deformation mode in each compression cycle and the standard deviations of the postbuckling load. Specifically, in the presence of a z+ magnetic field, the metamaterial lattice adopts a convex curvature even before any load is applied. Consequently, upon loading, a positive Poisson's ratio ($\nu_{max} = 3.41$) mode appears, indicating an expansion in the transverse direction relative to the applied axial strain. The critical load is 236 mN and the postbuckling slope turns positive with $S > 0$. Conversely, when subjected to a z− magnetic field, the metamaterial lattice exhibits an inward curvature before loading. A negative Poisson's ratio mode ($\nu_{max} = -2.64$) is observed, indicating a transverse contraction relative to the applied axial strain. The critical load is 256 mN and the postbuckling slope is positive with $S > 0$. In this mode, the slope undergoes a further increase when the compressive displacement exceeds 5.7 mm, which is caused by the contact of voxels.

To evaluate the stability of MSMs for long-cycle compression, fatigue tests are performed under three different magnetic field modes. The results indicate that the MSM lattice exhibits stable mechanical behaviors across all tested modes (Figures 3E–3G). Specifically, after 500 compression cycles, the MSM lattice retains 97%, 95%, and 94% of its maximum reactive force under the z+, z−, and no-magnetic-field modes, respectively.

Please cite this article in press as: Wang et al., Fluidic control programming for 3D magnetic soft metamaterials with reconfigurable mechanical behaviors, Cell Reports Physical Science (2024), https://doi.org/10.1016/j.xcrp.2024.102125

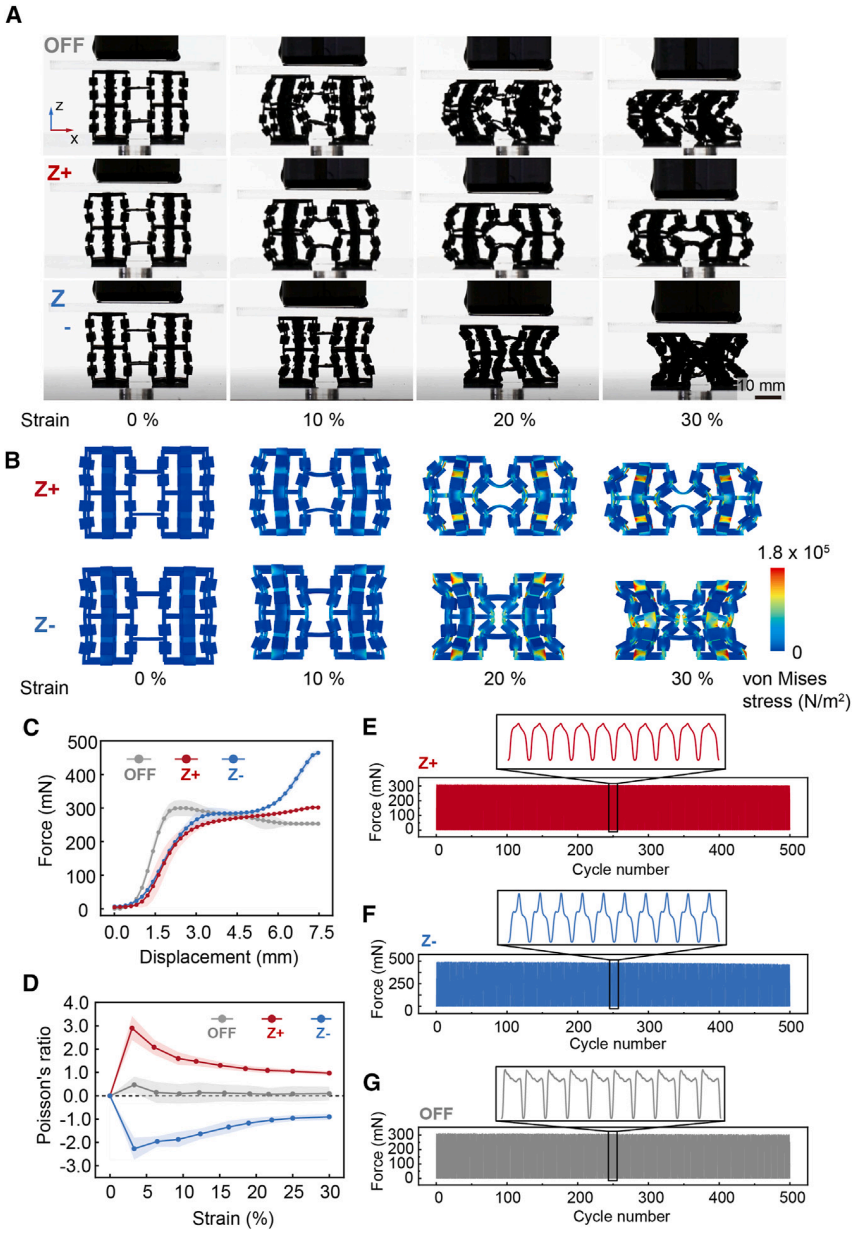

Figure 3. Magnetic soft metamaterial lattice with switchable Poisson's ratio

Magnetic fields are applied in z direction where the upward direction is defined as z+ and the downward direction is defined as z−.

(A) Images of 8-unit metamaterial lattice samples compressed in different magnetic field conditions. The black area above the sample is the linear slide, which applies the compressive load.

(B) Finite element analysis of 8-unit MSM lattice samples compressed in different magnetic field conditions.

(C) Force-displacement curve of 8-unit MSM lattice samples compressed in different magnetic field conditions. Each curve is the mean value of 3 compression tests, and the standard deviations are represented with shadows.

(D) Poisson's ratio-strain curve of 8-unit MSM lattice samples compressed in different magnetic field conditions. Each curve is the mean value of 3 compression tests, and the standard deviations are represented with shadows.

(E–G) Force-cycle number curves of MSM lattices in the fatigue test.

MSM lattice with reconfigurable orthotropic behaviors

With the multi-step injection and orientation strategy, 3D MSM structures with 64 voxels can be magnetized by four groups of orientations and therefore sixteen theoretical permutations and eight mechanical modes (after eliminating the duplication

Please cite this article in press as: Wang et al., Fluidic control programming for 3D magnetic soft metamaterials with reconfigurable mechanical behaviors, Cell Reports Physical Science (2024), https://doi.org/10.1016/j.xcrp.2024.102125

caused by symmetry) (Figure 4A). To demonstrate the capability of the 3D fluidic programming and reorientation for MSMs with various magnetization patterns, we fabricate MSM lattices with biaxial symmetric and anti-symmetric configurations (Figure 4B). Compared to the previously demonstrated metamaterial lattices, the magnetization mode is flipped between the x-z and y-z planes.

Verified through both simulation and compression testing, the symmetric MSM lattice shows either outward or inward curvatures on all four sides when subjected to magnetic fields of 50 mT in the z+ and z− scenarios (Figure 4C). In contrast, the biaxial anti-symmetric magnetic metamaterial lattice exhibits orthotropic deformation modes under the same compressional forces in magnetic fields of 50 mT in the z+ and z− scenarios (Figure 4D). Unlike the symmetric lattices, the anti-symmetric configuration shows different bending behaviors on each side, which leads to non-uniform deformation. This behavior is clearly visible in the compressional test images, where the deformation modes differ significantly from the symmetric counterpart. However, when the magnetic field is OFF, the biaxial anti-symmetric MSM lattice exhibits a similar buckling behavior to that of the symmetric metamaterial lattice, indicating that the primary differences arise due to the magnetization pattern under the influence of a magnetic field.

Specifically, when the magnetic field is turned on, the sample exhibits almost the same force-displacement curves in both z+ and z− magnetic fields (Figure 4E). When the magnetic field direction is z+, the sample shows an outward convexity in the y-z plane and an inward concavity in the x-z plane. When the magnetic field direction is z−, the sample is concave in the y-z plane and convex in the x-z plane. Upon loading, an expansion in the y-z plane (ν_{max} = 3.29) and contraction in the x-z plane (ν_{max} = −2.61) relative to the applied axial strain is observed (Figure 4F). Conversely, when subjected to a z− magnetic field (Figure 4G), the MSM lattice exhibits a negative Poisson's ratio mode in the y-z plane (ν_{max} = −2.76) and a positive Poisson's ratio in the x-z plane (ν_{max} = 3.44).

MSMs with programmable mechanical-based functions

The capability to generate multi-modal deformation allows us to achieve various functions with the metamaterial lattice, as shown in Figure 5. Our approach offers advantages for the development of soft robots that operate in confined spaces and require high compliance and precise actuation for miniaturization and safety. To demonstrate its instantaneous response and the advantages of wireless actuation using magnetic fields, we utilize one reconfigurable base unit as an in-tube soft robot. The base unit is inserted into a vertically placed glass tube with an inner diameter of 14 mm. Using a magnetic field, the base unit can be expanded or contracted in the transverse direction, thereby manipulating the frictional forces with the wall and enabling it to be anchored or released as desired.

As shown in Figure 5A, a cylindrical mass is placed on the top of the base unit. By switching the magnetic field to z−, the sample contracts, reducing friction and facilitating downward movement under the effect of gravity. Then, by switching the magnetic field to z+, it expands and instantaneously stops the downward movement of the load (Video S2). The weight of one base unit is 2.14 ± 0.1 g, and the carrying capability is evaluated with loads of 1.5, 2.5, 3.5, and 5.0 g, respectively (Figure 5B). In each case, the loads and the robot are released from the top, stopped in the middle, and then released again to fall to the bottom of the tube. Due to the instantaneous response to the magnetic field, a sudden stop can be achieved within a 0.01 s duration while the reconfigurable base unit drops through the tube.

Please cite this article in press as: Wang et al., Fluidic control programming for 3D magnetic soft metamaterials with reconfigurable mechanical behaviors, Cell Reports Physical Science (2024), https://doi.org/10.1016/j.xcrp.2024.102125

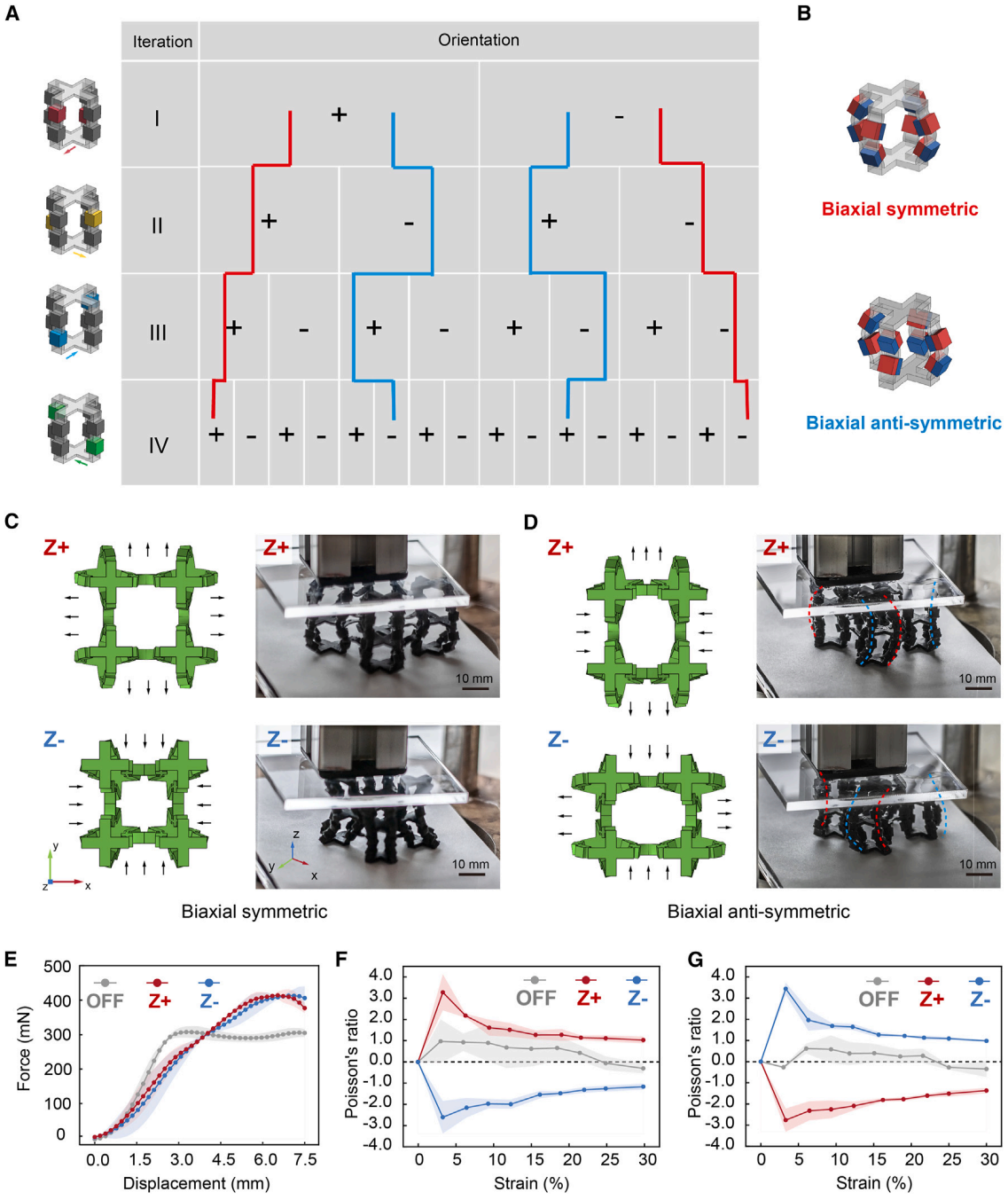

Figure 4. MSM lattice with reconfigurable orthotropic behaviors

Magnetic fields are applied in z direction where along the z axis is defined as z+ and the opposite direction along the z axis is defined as z−.

(A) Permutations of magnetization patterns for MSMs, where "+" is the direction represented by the colored arrow.

(B) Biaxial symmetric and biaxial anti-symmetric MSM base units.

(C) Simulation and experimental images for the deformation modes of biaxially symmetric lattices compressed in the presence of z− and z+ magnetic fields.

(D) Simulation and experimental images for the deformation modes of biaxially anti-symmetric lattices compressed in the presence of z− and z+ magnetic fields.

(E) Load-displacement curve of biaxial anti-symmetric magnetic metamaterial lattice.

(F) Poisson's ratio-strain curve of orthotropic metamaterial lattice in the x-z plane.

(G) Poisson's ratio-strain curve of orthotropic magnetic metamaterial lattice in y-z plane.

Please cite this article in press as: Wang et al., Fluidic control programming for 3D magnetic soft metamaterials with reconfigurable mechanical behaviors, Cell Reports Physical Science (2024), https://doi.org/10.1016/j.xcrp.2024.102125

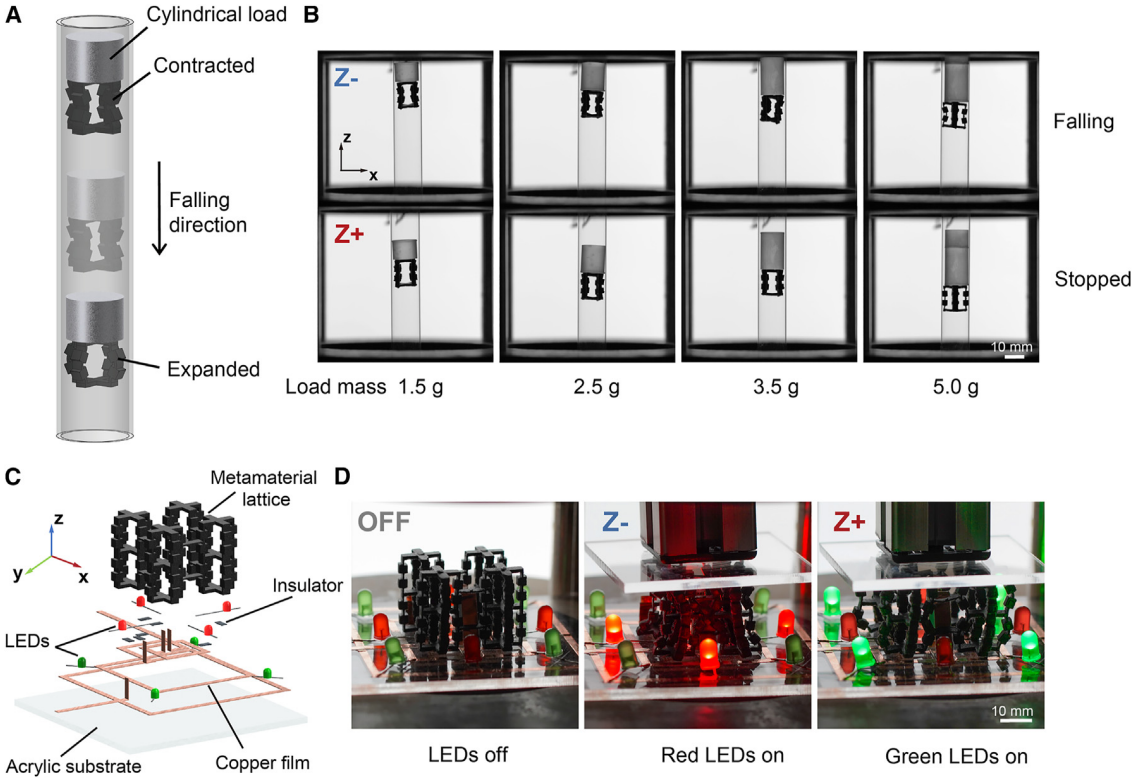

Figure 5. Functional demonstrations of the MSMs

Magnetic fields are applied in z direction where the upward direction is defined as z+ and the downward direction is defined as z−.

(A) Schematic of the programmable base unit used as a programmable load carrier.

(B) Images of the base unit stopping and releasing different masses by contracting and expanding in the presence of the magnetic field.

(C) Schematic design of metamaterial lattice as a reconfigurable soft electronic device.

(D) Metamaterial lattice-based soft electronic devices exhibit different electronic functions depending on the direction of applied magnetic fields of 50 mT.

We further demonstrate the capability of combining electronic components and circuitry with our multi-unit structure. An electrical circuit is developed with three modes of operation: switching on red light-emitting diodes (LEDs), switching on green LEDs, or turning off all LEDs. A metamaterial lattice sample with a magnetization pattern, depicted in Figure 2, is placed in the middle of the circuit, as shown in Figure 5C. The MSMs are then evaluated by functioning as a double-throw switch that can be activated by the magnetic-field-guided buckling in the designed circuit (Figure S10). When the material contracts, the red LEDs are activated, and the expansion of the material triggers the green LEDs (Figure 5D; Video S3). Similar results are also observed when pressing the MSMs above a 60 × 5 mm NdFeB disk magnet (Video S3). This result showcases that the magnetic metamaterial lattice can form parts of soft electronics and offer a high degree of programmability.

In conclusion, we develop a strategy to realize multi-modal deformation in 3D magnetic soft mechanical metamaterial structures through a voxelated fabrication methodology. Our approach achieves the magnetization of all voxels in a weak magnetic field through a multi-step injection strategy. The magnetic soft composite shows sensitive responses to the external magnetic field, resulting in a rapid switching between different mechanical behaviors such as positive/negative Poisson's ratio and orthotropic deformation. The reconfigurable MSMs also exhibit the ability

Please cite this article in press as: Wang et al., Fluidic control programming for 3D magnetic soft metamaterials with reconfigurable mechanical behaviors, Cell Reports Physical Science (2024), https://doi.org/10.1016/j.xcrp.2024.102125

to manipulate frictional forces in a glass tube. A soft electronic device with programmable functions is achieved, demonstrating the capabilities of the MSMs in electromagnetic applications. This work represents a step forward in the development of MSMs and holds great potential for future applications that require responsive and reconfigurable metamaterials.

To broaden the application scope, future investigations should consider integrating additional functionalities into MSMs, such as electrical conductivity and thermal responsiveness. Such advancements could transform the practical use of MSMs across diverse fields, for example in wearable technologies or other biomedical devices. Miniaturizing the MSMs to millimeters or even micrometers with more integrated units will also be important for future magnetic soft metamaterials with advanced functions.

EXPERIMENTAL PROCEDURES

Resource availability

Lead contact

Further information and requests for resources should be directed to and will be fulfilled by the lead contact, Zhuoyue Wang (z.wang01@umcg.nl).

Materials availability

This study did not generate new unique reagents. The materials generated in this study will be made available upon request.

Data and code availability

The data that support the findings in this study are available from the article and its supplemental information. All other relevant data are available from the lead contact upon reasonable request.

Preparation of magnetic composite

Before mixing, all the PrFeB particles (MQFPTM-16-7) were magnetized in an impulse magnetizer (IM-10-30, ASC SCIENTIFIC) at a 2 T magnetic field. The magnetic composite was prepared by blending PrFeB particles and Dragon Skin 30 (Smooth-On) in a ratio of 33 wt %. After thoroughly mixing at 2,800 rpm for 2 min, the blend was degassed inside a vacuum chamber for 5 min. The degassed mixture was then transferred into a 12 mL syringe and ready for injection.

Multi-step injection and weak field orientation

The multi-step injection process involved injecting uncured magnetic composites into one of the four main ports using a precision injection pump (NE-1000, ProSense B.V.) at a rate of 0.50 mL/s. After injection for each magnetization direction, the mold was transferred to the electromagnetic coil system and positioned for specific magnetization orientations. Then, an 80 mT magnetic field was applied for 5 s to orientate the particles. Subsequently, the mold was moved to a heating platform and maintained at a temperature of 80°C for 15 min to ensure full curing of the magnetic composites. This injection procedure was repeated for all magnetization groups successively. Finally, the composite was also injected into the connecting channels and cured without orientation in the electromagnetic field.

In situ mechanical tests

An *in situ* mechanical test system as depicted in Figure S8 was established including a stepper motor (NEMA-17, Adafruit Industries), a load cell sensor (YZC-131-1kg, Guangzhou Electrical Measuring Instruments Factory), and a microcontroller (Arduino

Mega 2560 Rev3). During the tests, vertical magnetic fields (z direction) were applied. In all conditions, the stepper motor moved at the speed of 1 mm/s, cycling between compressing distances of 6.5 mm for the base units and 7.5 mm for the multi-unit metamaterial lattice. To measure the Poisson's ratio, a DSLM camera (ICLE-7C, Sony) was placed directly in front of the sample to take a 120 fps video of the tests, and Fiji[51] was used to calculate the transverse deformation.

Fatigue tests are also performed with the *in situ* mechanical test setup. Samples of the MSM lattice were subjected to 500 compression cycles in the setup depicted in Figure S8. The loading and unloading rates were maintained at 1 mm/s, with a total displacement of 7.5 mm for each cycle.

Finite element analysis

For the designs presented in Figures 1 and 3, deformations in the presence of external magnetic fields were simulated using the Solid Mechanics and Magnetic Fields, No Currents module in COMSOL Multiphysics 5.4. The material is defined as linear elastic according to the mechanical experiments (Figure 1F), with a Young's modulus E = 485 kPa. The simulations applied a uniform external magnetic field $\boldsymbol{B}$ = 50 mT. The boundary conditions and the configuration of q are illustrated in Figure S11. Details on the material properties and mesh parameters used are provided in Table S2. For multi-unit lattice structures, a magnetic torque was modeled using surface loads with equal magnitude and opposite directions on each voxel. The area load q is calculated as Equation 3:

$$q = \frac{mB\sin\theta}{Ad} = \frac{MV_{vox}B\sin\theta}{Ad}, \qquad \text{(Equation 3)}$$

where q is the area load (N/m^2), m is the magnetic moment (A/m^2), B is the flux density of the magnetic field applied (T), θ is the angle between the magnetization direction ($\boldsymbol{M}$) of the voxel and the direction of the externally applied magnetic field ($\boldsymbol{B}$), A is the area that the load acts on (m^2), and d is the distance between two opposite loads (m). M is the magnetization of the composite materials, which is measured at 8.7 kA/m with a Hall-effect-based setup (Note S1). V_{vox} is the volume of the voxel (m^3).

Material mechanical characterization

The mechanical characterization was conducted using a texture analyzer (CT3, AMETEK GmbH B.U. Brookfield). Standardized testing samples made of Dragon Skin 30 and the magnetic composites were subjected to axis tensile tests as per ASTM standard tests. The loading speed for the tests was set to 1 mm/s, and the testing range was set to 200% of strain. Nominal stress-strain curves are provided in Figure 1F.

SUPPLEMENTAL INFORMATION

Supplemental information can be found online at https://doi.org/10.1016/j.xcrp.2024.102125.

ACKNOWLEDGMENTS

This work is supported by the Europe Research Council (ERC) under the European Union's Horizon 2020 Research and Innovation program under grant agreement #866494-project MAESTRO and with financial support from China Scholarship Council (CSC, file no. 202106180026).

Please cite this article in press as: Wang et al., Fluidic control programming for 3D magnetic soft metamaterials with reconfigurable mechanical behaviors, Cell Reports Physical Science (2024), https://doi.org/10.1016/j.xcrp.2024.102125

AUTHOR CONTRIBUTIONS

Ideation, Z.W. and V.K.V.; experimental investigation, Z.W.; writing and editing, Z.W., V.K.V., and S.M.; project supervision, S.M. and V.K.V.; funding acquisition, S.M and Z.W.

DECLARATION OF INTERESTS

The authors declare no competing interests.

Received: April 11, 2024
Revised: June 25, 2024
Accepted: July 5, 2024
Published: July 29, 2024

REFERENCES

1. Zhang, H., Wu, J., Fang, D., and Zhang, Y. (2021). Hierarchical mechanical metamaterials built with scalable tristable elements for ternary logic operation and amplitude modulation. Sci. Adv. *7*, eabf1966. https://doi.org/10.1126/sciadv.abf1966.

2. Montgomery, S.M., Wu, S., Kuang, X., Armstrong, C.D., Zemelka, C., Ze, Q., Zhang, R., Zhao, R., and Qi, H.J. (2021). Magneto-Mechanical Metamaterials with Widely Tunable Mechanical Properties and Acoustic Bandgaps. Adv. Funct. Mater. *31*, 2005319. https://doi.org/10.1002/adfm.202005319.

3. Kadic, M., Milton, G.W., van Hecke, M., and Wegener, M. (2019). 3D metamaterials. Nat. Rev. Phys. *1*, 198–210. https://doi.org/10.1038/s42254-018-0018-y.

4. Lakes, R. (1987). Foam Structures with a Negative Poisson's Ratio. Science *235*, 1038–1040. https://doi.org/10.1126/science.235.4792.1038.

5. Babaee, S., Shim, J., Weaver, J.C., Chen, E.R., Patel, N., and Bertoldi, K. (2013). 3D Soft Metamaterials with Negative Poisson's Ratio. Adv. Mater. *25*, 5044–5049. https://doi.org/10.1002/adma.201301986.

6. Bertoldi, K., Reis, P.M., Willshaw, S., and Mullin, T. (2010). Negative Poisson's Ratio Behavior Induced by an Elastic Instability. Adv. Mater. *22*, 361–366. https://doi.org/10.1002/adma.200901956.

7. Shi, X., Zhu, Y., Fan, X., Wu, H.A., Wu, P., Ji, X., Chen, Y., and Liang, J. (2022). An auxetic cellular structure as a universal design for enhanced piezoresistive sensitivity. Matter *5*, 1547–1562. https://doi.org/10.1016/J.MATT.2022.02.022.

8. Hewage, T.A.M., Alderson, K.L., Alderson, A., and Scarpa, F. (2016). Double-Negative Mechanical Metamaterials Displaying Simultaneous Negative Stiffness and Negative Poisson's Ratio Properties. Adv. Mater. *28*, 10323–10332. https://doi.org/10.1002/adma.201603959.

9. Correa, D.M., Klatt, T., Cortes, S., Haberman, M., Kovar, D., and Seepersad, C. (2015). Negative stiffness honeycombs for recoverable shock isolation. Rapid Prototyp. J. *21*, 193–200. https://doi.org/10.1108/RPJ-12-2014-0182.

10. Wu, L., Li, B., and Zhou, J. (2016). Isotropic Negative Thermal Expansion Metamaterials. ACS Appl. Mater. Interfaces *8*, 17721–17727. https://doi.org/10.1021/ACSAMI.6B05717.

11. Qu, J., Kadic, M., Naber, A., and Wegener, M. (2017). Micro-Structured Two-Component 3D Metamaterials with Negative Thermal-Expansion Coefficient from Positive Constituents. Sci. Rep. *7*, 40643–40648. https://doi.org/10.1038/srep40643.

12. Xu, X., Zhang, Q., Hao, M., Hu, Y., Lin, Z., Peng, L., Wang, T., Ren, X., Wang, C., Zhao, Z., et al. (2019). Double-negative-index ceramic aerogels for thermal superinsulation. Science *363*, 723–727. https://doi.org/10.1126/science.aav7304.

13. Frenzel, T., Kadic, M., and Wegener, M. (2017). Three-dimensional mechanical metamaterials with a twist. Science *358*, 1072–1074. https://doi.org/10.1126/science.aao4640.

14. Xin, X., Liu, L., Liu, Y., Leng, J., Xin, X., Liu, L., Liu, Y., and Leng, J. (2020). 4D Printing Auxetic Metamaterials with Tunable, Programmable, and Reconfigurable Mechanical Properties. Adv. Funct. Mater. *30*, 2004226. https://doi.org/10.1002/ADFM.202004226.

15. Ren, Z., Ji, L., Tao, R., Chen, M., Wan, Z., Zhao, Z., and Fang, D. (2021). SMP-based multi-stable mechanical metamaterials: From bandgap tuning to wave logic gates. Extreme Mech. Lett. *42*, 101077. https://doi.org/10.1016/j.eml.2020.101077.

16. Yang, C., Boorugu, M., Dopp, A., Ren, J., Martin, R., Han, D., Choi, W., and Lee, H. (2019). 4D printing reconfigurable, deployable and mechanically tunable metamaterials. Mater. Horiz. *6*, 1244–1250. https://doi.org/10.1039/C9MH00302A.

17. Tariq, A., Arif, Z.U., Khalid, M.Y., Hossain, M., Rasool, P.I., Umer, R., and Ramakrishna, S. (2023). Recent Advances in the Additive Manufacturing of Stimuli-Responsive Soft Polymers. Adv. Eng. Mater. *25*, 2301074. https://doi.org/10.1002/ADEM.202301074.

18. Arif, Z.U., Khalid, M.Y., Tariq, A., Hossain, M., and Umer, R. (2024). 3D printing of stimuli-responsive hydrogel materials: Literature review and emerging applications. Giant *17*, 100209. https://doi.org/10.1016/J.GIANT.2023.100209.

19. Zou, B., Liang, Z., Zhong, D., Cui, Z., Xiao, K., Shao, S., and Ju, J. (2023). Magneto-thermomechanically reprogrammable mechanical metamaterials. Adv. Mater. *35*, e2207349. https://doi.org/10.1002/adma.202207349.

20. Gu, H., Boehler, Q., Ahmed, D., and Nelson, B.J. (2019). Magnetic quadrupole assemblies with arbitrary shapes and magnetizations. Sci. Robot. *4*, eaax8977. https://doi.org/10.1126/SCIROBOTICS.AAX8977.

21. Kim, Y., and Zhao, X. (2022). Magnetic Soft Materials and Robots. Chem. Rev. *122*, 5317–5364. https://doi.org/10.1021/ACS.CHEMREV.1C00481.

22. Zhang, J., Ren, Z., Hu, W., Soon, R.H., Yasa, I.C., Liu, Z., and Sitti, M. (2021). Voxelated three-dimensional miniature magnetic soft machines via multimaterial heterogeneous assembly. Sci. Robot. *6*, eabf0112. https://doi.org/10.1126/scirobotics.abf0112.

23. Venkiteswaran, V.K., Samaniego, L.F.P., Sikorski, J., and Misra, S. (2019). Bio-Inspired Terrestrial Motion of Magnetic Soft Millirobots. IEEE Rob. Autom. Lett. *4*, 1753–1759. https://doi.org/10.1109/lra.2019.2898040.

24. Jackson, J.A., Messner, M.C., Dudukovic, N.A., Smith, W.L., Bekker, L., Moran, B., Golobic, A.M., Pascall, A.J., Duoss, E.B., Loh, K.J., and Spadaccini, C.M. (2018). Field responsive mechanical metamaterials. Sci. Adv. *4*, u6419. https://doi.org/10.1126/sciadv.aau6419.

25. Wu, S., Eichenberger, J., Dai, J., Chang, Y., Ghalichechian, N., and Zhao, R.R. (2022). Magnetically Actuated Reconfigurable Metamaterials as Conformal Electromagnetic Filters. Adv. Intell. Syst. *4*, 2200106. https://doi.org/10.1002/AISY.202200106.

26. Ma, C., Chang, Y., Wu, S., and Zhao, R.R. (2022). Deep Learning-Accelerated Designs of Tunable Magneto-Mechanical Metamaterials. ACS Appl. Mater. Interfaces. Published online July 14, 2022. https://doi.org/10.1021/ACSAMI.2C09052.

27. Chen, T., Pauly, M., and Reis, P.M. (2021). A reprogrammable mechanical metamaterial with stable memory. Nature *589*, 386–390. https://doi.org/10.1038/s41586-020-03123-5.

28. Khalid, M.Y., Arif, Z.U., Tariq, A., Hossain, M., Ahmed Khan, K., and Umer, R. (2024). 3D printing of magneto-active smart materials for advanced actuators and soft robotics applications. Eur. Polym. J. *205*, 112718. https://doi.org/10.1016/J.EURPOLYMJ.2023.112718.

29. Wu, S., Hu, W., Ze, Q., Sitti, M., and Zhao, R. (2020). Multifunctional magnetic soft composites: a review. Multifunct. Mater. *3*, 042003. https://doi.org/10.1088/2399-7532/ABCB0C.

30. Qi, Z., Zhou, M., Li, Y., Xia, Z., Huo, W., Huang, X., Qi, Z., Zhou, M., Li, Y., Xia, Z., et al. (2021). Reconfigurable Flexible Electronics Driven by Origami Magnetic Membranes. Adv. Mater. Technol. *6*, 2001124. https://doi.org/10.1002/ADMT.202001124.

31. Ma, C., Wu, S., Ze, Q., Kuang, X., Zhang, R., Qi, H.J., and Zhao, R. (2021). Magnetic Multimaterial Printing for Multimodal Shape Transformation with Tunable Properties and Shiftable Mechanical Behaviors. ACS Appl. Mater. Interfaces *13*, 12639–12648. https://doi.org/10.1021/ACSAMI.0C13863.

32. Huang, H.-W., Sakar, M.S., Petruska, A.J., Pané, S., and Nelson, B.J. (2016). Soft micromachines with programmable motility and morphology. Nat. Commun. *7*, 12263. https://doi.org/10.1038/ncomms12263.

33. Kim, Y., Yuk, H., Zhao, R., Chester, S.A., and Zhao, X. (2018). Printing ferromagnetic domains for untethered fast-transforming soft materials. Nature *558*, 274–279. https://doi.org/10.1038/S41586-018-0185-0.

34. Kim, Y., Parada, G.A., Liu, S., and Zhao, X. (2019). Ferromagnetic soft continuum robots. Sci. Robot. *4*, eaax7329. https://doi.org/10.1126/scirobotics.aax7329.

35. Hu, W., Lum, G.Z., Mastrangeli, M., and Sitti, M. (2018). Small-scale soft-bodied robot with multimodal locomotion. Nature *554*, 81–85. https://doi.org/10.1038/nature25443.

36. Wang, C., Mzyk, A., Schirhagl, R., Misra, S., and Venkiteswaran, V.K. (2023). Biocompatible Film-Coating of Magnetic Soft Robots for Mucoadhesive Locomotion. Adv. Mater. Technol. *8*, 2201813. https://doi.org/10.1002/ADMT.202201813.

37. Wei, Z.Y., Guo, Z.V., Dudte, L., Liang, H.Y., and Mahadevan, L. (2013). Geometric Mechanics of Periodic Pleated Origami. Phys. Rev. Lett. *110*, 215501. https://doi.org/10.1103/PhysRevLett.110.215501.

38. Lv, C., Krishnaraju, D., Konjevod, G., Yu, H., and Jiang, H. (2014). Origami based Mechanical Metamaterials. Sci. Rep. *4*, 5979. https://doi.org/10.1038/srep05979.

39. Overvelde, J.T.B., de Jong, T.A., Shevchenko, Y., Becerra, S.A., Whitesides, G.M., Weaver, J.C., Hoberman, C., and Bertoldi, K. (2016). A three-dimensional actuated origami-inspired transformable metamaterial with multiple degrees of freedom. Nat. Commun. *7*, 10929. https://doi.org/10.1038/ncomms10929.

40. Surjadi, J.U., Zhou, Y., Huang, S., Wang, L., Li, M., Fan, S., Li, X., Zhou, J., Lam, R.H.W., Wang, Z., and Lu, Y. (2022). Lightweight, ultra-tough, 3D-architected hybrid carbon microlattices. Matter *5*, 4029–4046. https://doi.org/10.1016/J.MATT.2022.08.010.

41. Lee, H., Jang, Y., Choe, J.K., Lee, S., Song, H., Lee, J.P., Lone, N., and Kim, J. (2020). 3D-printed programmable tensegrity for soft robotics. Sci. Robot. *5*, eaay9024. https://doi.org/10.1126/SCIROBOTICS.AAY9024.

42. Gong, X., Tan, K., Deng, Q., and Shen, S. (2020). Athermal Shape Memory Effect in Magnetoactive Elastomers. ACS Appl. Mater. Interfaces *12*, 16930–16936. https://doi.org/10.1021/acsami.0c01453.

43. Testa, P., Style, R.W., Cui, J., Donnelly, C., Borisova, E., Derlet, P.M., Dufresne, E.R., Heyderman, L.J., Testa, P., Cui, J., et al. (2019). Magnetically Addressable Shape-Memory and Stiffening in a Composite Elastomer. Adv. Mater. *31*, 1900561. https://doi.org/10.1002/ADMA.201900561.

44. Kim, J., Chung, S.E., Choi, S.-E., Lee, H., Kim, J., and Kwon, S. (2011). Programming magnetic anisotropy in polymeric microactuators. Nat. Mater. *10*, 747–752. https://doi.org/10.1038/nmat3090.

45. Zhang, Y., Pan, C., Liu, P., Peng, L., Liu, Z., Li, Y., Wang, Q., Wu, T., Li, Z., Majidi, C., and Jiang, L. (2023). Coaxially printed magnetic mechanical electrical hybrid structures with actuation and sensing functionalities. Nat. Commun. *14*, 4428–4515. https://doi.org/10.1038/S41467-023-40109-Z.

46. Khalid, M.Y., Arif, Z.U., Noroozi, R., Hossain, M., Ramakrishna, S., and Umer, R. (2023). 3D/4D printing of cellulose nanocrystals-based biomaterials: Additives for sustainable applications. Int. J. Biol. Macromol. *251*, 126287. https://doi.org/10.1016/J.IJBIOMAC.2023.126287.

47. Alapan, Y., Karacakol, A.C., Guzelhan, S.N., Isik, I., and Sitti, M. (2020). Reprogrammable shape morphing of magnetic soft machines. Sci. Adv. *6*, eabc6414. https://doi.org/10.1126/sciadv.abc6414.

48. Song, H., Lee, H., Lee, J., Choe, J.K., Lee, S., Yi, J.Y., Park, S., Yoo, J.-W., Kwon, M.S., and Kim, J. (2020). Reprogrammable Ferromagnetic Domains for Reconfigurable Soft Magnetic Actuators. Nano Lett. *20*, 5185–5192. https://doi.org/10.1021/acs.nanolett.0c01418.

49. Chen, W.-F., and Atsuta, T. (2008). Theory of Beam-Columns (J. Ross Publishing).

50. Coulais, C., Overvelde, J.T.B., Lubbers, L.A., Bertoldi, K., and Van Hecke, M. (2015). Discontinuous Buckling of Wide Beams and Metabeams. https://doi.org/10.1103/PhysRevLett.115.044301.

51. Schindelin, J., Arganda-Carreras, I., Frise, E., Kaynig, V., Longair, M., Pietzsch, T., Preibisch, S., Rueden, C., Saalfeld, S., Schmid, B., et al. (2012). Fiji: an open-source platform for biological-image analysis. Nat. Methods *9*, 676–682. https://doi.org/10.1038/NMETH.2019.